Journal of Geochemical Exploration 185 (2018) 1–13

Contents lists available at ScienceDirect

Journal of Geochemical Exploration

journal homepage: www.elsevier.com/locate/gexplo

Decoding fjord water contribution and geochemical processes in the Aysen thermal springs (Southern Patagonia, Chile)

Angello Negri[a], Linda Daniele[a,*], Diego Aravena[a], Mauricio Muñoz[a], Antonio Delgado[b], Diego Morata[a]

[a] Department of Geology and Andean Geothermal Center of Excellence (CEGA, FONDAP-CONYCIT 15090013), FCFM, University of Chile, 8370450 Santiago, Chile.
[b] Laboratorio de Biogeoquímica de Isótopos Estables, Estación Experimental del Zaidín (CSIC), 18008 Armilla, Granada, Spain.

ARTICLE INFO

Keywords:
Thermal waters
Fjord-water mixing
Silicate weathering
Multivariate statistical analysis

ABSTRACT

The Aysen region, located in Southern Patagonia, Chile (43°38′S to 49°16′S) has optimum conditions for the formation of geothermal systems: Magmatic processes, abundant rainfall and active faults systems. In fact, several thermal springs emerge in coastal and inland areas of the Aysen region. Thermal springs in the coastal areas are spatially related to the Liquiñe-Ofqui Fault System (LOFS), a major strike-slip fault system that runs along the southern segment of the Southern Volcanic Zone, and could be controlling groundwater circulation. Despite the existence of literature regarding the composition of thermal springs, they do not elucidate the origin of thermal waters, the source of their chemical components nor have their hydrogeochemical processes been investigated. This knowledge will provide a useful tool for exploration of geothermal resources in the Aysen region.

Sixteen thermal waters, three fjord waters, and three meteoric water samples were collected and analysed for major-minor ions, some trace elements (B, Li) and stable isotopes of δ^2H and $\delta^{18}O$. Classic geochemical tools (i.e.: ratio of elements, ion vs chloride content), Hierarchical Cluster Analysis (HCA) and Factorial Analysis (FA) suggest there are three water groups (G1, G2 and G3). G1 and G3 are Na—Cl type coastal thermal springs with electrical conductivity (EC) above 1000 μS/cm and mostly neutral pH (6.4 to 8.4). G1 has the highest average concentrations of Cl^-, SO_4^{2-}, Na^+, Ca^{2+} while G3 has the highest values T°, SiO_2, HCO_3^-, Li, B. The G2 samples are from Aysen inland areas, have EC below 1000 μS/cm, slightly alkaline pH (7.9 to 9.6) and are Na-Cl-HCO_3 type with higher average values of T°, SiO_2, HCO_3^- and Li than G1.

Factorial analysis indicates that two factors explain 82.1% of the total dataset variance. Factor 1 is formed by Cl^-, SO_4^{2-}, Na^+, Ca^{2+}, Li and B, which we associated with fjord water mixing processes. The factor 2 formed by T°, SiO_2, HCO_3^-, Li and B might be interpreted as: i) silicate weathering from the North Patagonian Batholith and ii) volatile elements transported through high temperature vapours from a volcanic degassing source. These two components which could interact and overlap are address as “magmatic-hydrothermal” in this work. The factorial scores distribution is consistent with the HCA suggesting that fjord water mixing is the dominant geochemical process for G1 samples while G2 samples are influenced by magmatic-hydrothermal fluids. The G3 thermal waters show both processes with a greater influence of magmatic-hydrothermal fluids. The calculated saline factor (3.4% to 42.3%) supports fjord water mixing processes as one of the dominant processes affecting the coastal thermal spring's composition.

The stable isotopic data (δ^2H and $\delta^{18}O$) fall in the local meteoric water line (LMWL), suggesting current recharge and limited oxygen isotopic exchange during rock-dissolution processes. This could indicate short residence times and/or abundant contribution of actual meteoric water at shallow depths.

1. Introduction

During the last decades, several studies have been undertaken to analyze the chemical and isotopic composition of geothermal fluids. That studies have allowed a better understanding of factors that are influencing its hydrogeochemical features, such as the nature of the initial recharge waters, the residence times, the water-rock interactions and water mixing processes (e.g. Dotsika, 2015; Dotsika et al., 2010; Ellis and Mahon, 1964, 1977; Giggenbach, 1988, 1995; Millot et al., 2012; Vengosh et al., 2002). Research on coastal geothermal systems

* Corresponding author.
E-mail address: ldaniele@ing.uchile.cl (L. Daniele).

https://doi.org/10.1016/j.gexplo.2017.10.026
Received 12 May 2017; Received in revised form 10 October 2017; Accepted 26 October 2017
Available online 11 November 2017
0375-6742/

have been performed worldwide, examples include Iceland (e.g. Arnórsson et al., 1983a, 1983b), New Zealand (e.g. Millot et al., 2012; Reyes et al., 2010), Greece (e.g. Dotsika, 2015; Dotsika et al., 2010; Duriez et al., 2008), and Turkey (e.g. Vengosh et al., 2002). Thermal fluids along coastline are mainly Na−Cl type and generally brackish to saline because seawater masks the original ionic composition of the fluids (Dotsika, 2015).

In Chile, several authors have inventoried thermal springs (Hauser, 1997; Pérez, 1999), studied the chemical and isotopic composition of thermal fluids (Benavente et al., 2013, 2016; Capaccioni et al., 2011; Cortecci et al., 2005; Pérez, 1999; Ray et al., 2009; Risacher et al., 2011; Sepúlveda et al., 2004, 2007; Tassi et al., 2005, 2010) and characterized the interplay between volcanism and structural control on geochemistry of thermal waters (Alam et al., 2010; Pérez-Flores et al., 2016; Sanchez-Alfaro et al., 2016; Sánchez et al., 2013; Tardani et al., 2016). Previous studies have: i) Reported seawater influence in thermal waters of the south of Chile (37° − 45°S), including only two samples from the Aysen region (Risacher et al., 2011); ii) carried out a description and hydrogeochemical classification of some thermal springs (Hauser, 1989, 1997; Risacher et al., 2011); and iii) have discussed the general hydrogeological conditions (transmissivity and storage) through well data and structural features of geological units (Sernageomin, 2011).

The Aysen region has optimum conditions for the formation of geothermal systems: the existence of magmatic processes (D'Orazio et al., 2003; Gutiérrez et al., 2005; Hervei et al., 1995; Lahsen et al., 1994), abundant rainfall (~1200 mm/year) and active faults systems (Arancibia et al., 1999; Cembrano et al., 2002) that allow the deep circulation and rising of fluids. The region has 16 identified thermal springs distributed along 310 km; from Puerto Raul Marin Balmaceda (43°50′S) to Lago General Carrera (46°36′S), in both coastal and inland areas (Fig. 1). Thermal fluids generally outflow from fractures along the North Patagonian Batholith (NPB), an intrusive host rock, indicating that structural features are controlling the thermal springs and aquifer storage capacity must be controlled by fluids circulation through fractured zones. This is supported by strong interaction between recent tectonic activity and fluid flow in the LOFS (Legrand et al., 2011).

In this study, new data from thermal, meteoric and fjord waters in the Aysen region are analysed to elucidate the nature and origin of the geothermal fluids. We also identify and quantify the main hydrogeological processes driving their chemical behavior. This paper provides new information of thermal waters related to geothermal systems in Southern Patagonia, moreover, the Aysen region has a promising geothermal potential (Aravena et al., 2016) and these data can be used to take further steps towards the exploration and exploitation of Andean geothermal reservoirs.

2. Geological and hydrogeological setting

The Aysen region (43°38′S to 49°16′S), in the Southern-most Zone of Chile, is located in an active plate margin associated with northeast-directed subduction of the oceanic plates under the South American continental plate. At around 46°S, the active Chile Ridge intersect the continental margin, separating the Nazca oceanic plate from Antarctic oceanic plate, determining the existence of the Taitao triple-junction. Nowadays, one segment of the active oceanic spreading ridge (Chile Ridge) is being subducted under the General Carrera Lake, generating a very hot young oceanic lithosphere beneath the South American plate as a result of active opening of the slab (Lagabrielle et al., 2004).

Late subduction is evidenced by a series of Quaternary stratovolcanoes and monogenetic cones located along fractures related to the LOFS, considered as a major intra-arc dextral strike-slip fault system, which runs from the 39°S to 46°S latitude (Cembrano et al., 1996, 2002; Cembrano and Hervé, 1993; Cembrano and Lara, 2009; Niemeyer et al., 1984). The main lineaments are represented by two NNE trending straight segments and four NE en-échelon-trending segments in the Aysen region (Cembrano and Hervé, 1993) (Fig. 1). Structures in the study area coincide with an extensive fjord network formed by narrow channels and several islands, which separate the mainland from the adjacent Pacific Ocean (Bertrand et al., 2012). The geology along the LOFS is dominated by NPB, a plutonic rock belt of 1000 km long and 200 km wide, emplaced during discrete episodes of magmatism from Late Jurassic to Late Cenozoic times (Pankhurst et al., 1999; Suárez and De la Cruz, 2001) (Fig. 1). The igneous lithology of the batholith is mainly composed of hornblende-biotite granodiorite and tonalite, where the igneous suite is typically metaluminous and calc-alkaline (Pankhurst et al., 1999).

Two metamorphic complexes crop out west and east of the NPB (Fig. 1). The western unit is the Chonos Metamorphic Complex (CMC), which has been interpreted as an accretionary complex (Hervé et al., 1988) deposited during Late Triassic times (Fang et al., 1998; Herve and Fanning, 2001). It is mainly composed by metaturbidites, with less presence of metabasites, metachert, and green schist (Herve et al., 1981; Willner et al., 2000). The eastern unit is the Eastern Andean Metamorphic Complex (EAMC), which is composed of metasandstones, metapelite-schists, metaconglomerates, metacherts, and marble (Hervé et al., 2008; Ramirez-Sánchez et al., 2005) from an upper Devonian-early Carboniferous depositional age (Herve et al., 2003). The EAMC underlies in disconformity and angular unconformity with the Mesozoic-Cenozoic volcanic-sedimentary sequence located mainly in the back-arc domain (De la Cruz and Suárez, 2006; Niemeyer et al., 1984).

The fluvial and glaciofluvial unconsolidated deposits of Holocene-Pleistocene ages are the most important hydrogeological units generally located next to coastal villages, mainly in valleys or terraces (Sernageomin, 2011). In addition, the geological units with high permeability in eastern locations are restricted to fluvial deposits of low thickness in the edges of the active streambeds (Sernageomin, 2011). On the other hand, the hydrogeological information of igneous, metamorphic, and volcanic-sedimentary units cropping out in the most part of the region is still scarce due to lack of studies and exploration wells water resource, in spite of this, Sernageomin (2011) considered them low permeability units.

3. Methods

3.1. Sampling and analytical procedures

During the 2015 summer-winter period we sampled a set of 16 thermal springs, along with 3 samples of fjord water and 3 samples of rain water. Temperature, electrical conductivity (EC), redox potential (Eh) and pH were measured in situ (Table 1). Water samples were filtered using 0.45 μm Millipore filters, unacidified samples were collected for anion analysis, and acidified samples (with Suprapur® Nitric acid) for cations and trace elements analysis. Additionally, unfiltered samples were collected for isotopic analysis. All samples were stored in pre-cleaned polyethylene bottles at 4 °C.

Major, minor and trace elements were analysed in the laboratories Andean Geothermal Centre of Excellence (CEGA). Cl^-, SO_4^{2-}, F^-, Br^-, and NO_3^- contents were determined by Ion Chromatography (IC, Dionex ICS 2100) with a detection limit of 0.03 mg/l. Na^+, K^+, Ca^{2+}, and Mg^{2+} were measured by Atomic Absorption Spectrophotometry (AAS, Perkin-Elmer Pinaacle 900F) with detection limits of 0.05, 0.12, 0.15 and 0.003 mg/l, respectively. B and Li contents were determined by Inductively Coupled Plasma Mass Spectrometry (ICP-MS, Thermo iCAP Q) with detection limits of 0.20 and 0.02 ppb, respectively. The SiO_2 contents were analysed by Portable Photometer (Hanna HI96705) with a precision of ± 3%, and HCO_3^- concentration were determined by Volumetric Titration using Giggenbach and Goguel (1989) method. Isotopes analysis was carried out in the *Estación Experimental de Zaidín* (CSIC, Spain). The $\delta^{18}O$ and $\delta^{2}H$ were analysed by Finnigan Delta Plus XL mass spectrometer. Oxygen isotopes were measured using the CO_2-H_2O equilibration method (Epstein and Mayeda, 1953). Hydrogen

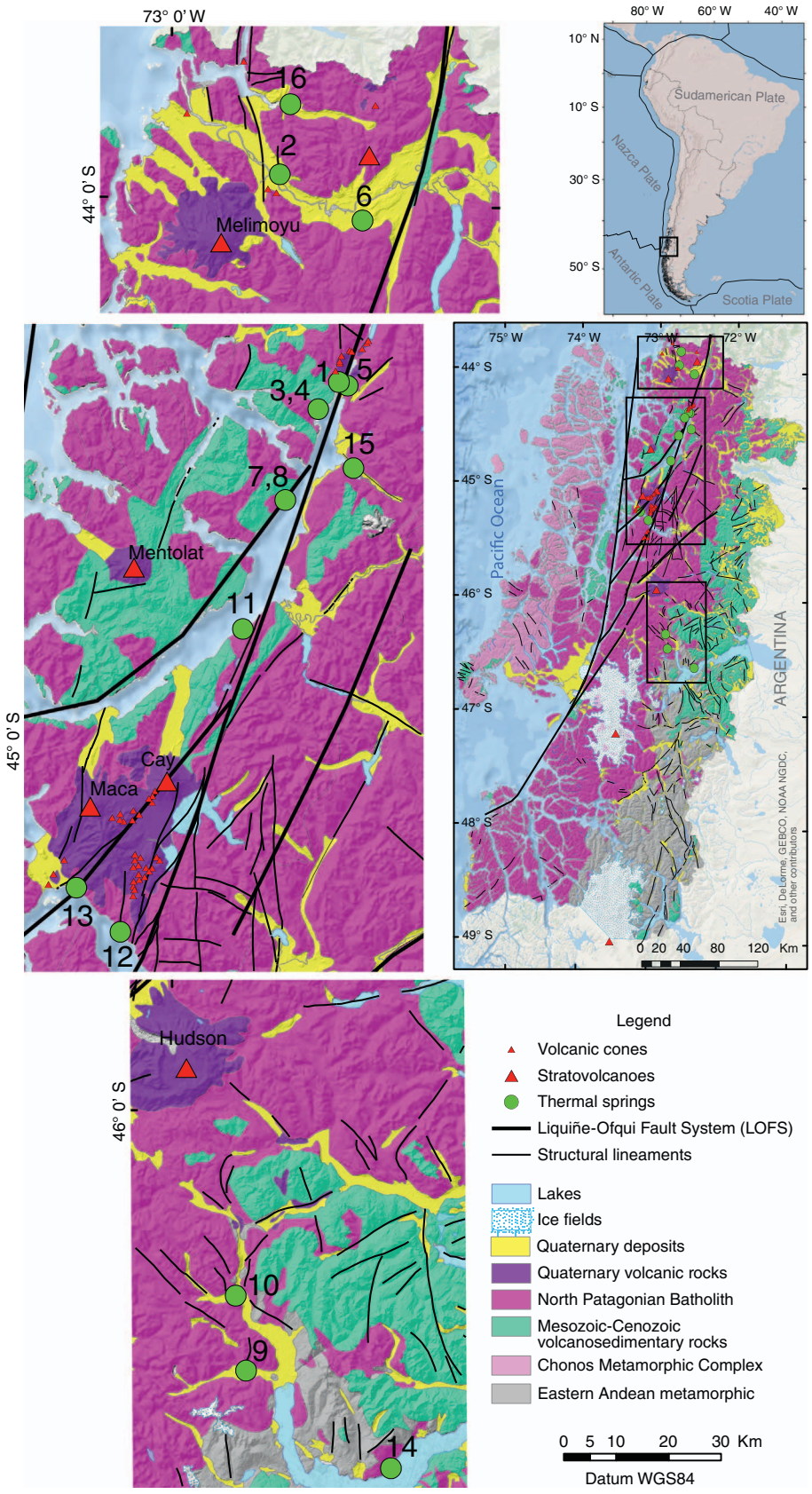

Fig. 1. Geological map of the Aysen region, southern Chile. The location of the thermal springs, superficial manifestations of volcanic activity, main traces of LOFZ and secondary lineaments are shown.
Modified of Sernageomin (2010).

isotopic ratio were determined from H_2 after the reaction of 10 ml of water with metallic zinc at 500 °C (Coleman et al., 1982). The experimental error was ± 0.1% and ± 1.1% for $\delta^{18}O$ and $\delta^{2}H$ values, respectively.

3.2. Geostatistical methods

Multivariate statistical methods have been widely used in several studies to identify geochemical clusters and to establish the main

Table 1
Chemical and isotopic analysis of meteoric (MW), thermal and fjord water (F_jW) samples from Aysen region.

Sample	Thermal Springs	North	East	Altitude	F_jW %	pH	EC	T°	Eh	SiO_2	Cl^-	SO_4^{2-}	HCO_3^-
ID		WGS84 18°S		m.a.s.l.			[μS/cm]	[°C]	[mV]	[mg/l]			
1	Gañote	5,084,758	691,509	3	42.3	7.5	11,660	60.9	− 53.0	109.00	3504.37	177.54	52.88
2	Puerto Bonito	5,130,766	681,919	37	–	9.6	360	42.0	− 219.0	86.00	36.84	28.94	53.90
3	Puyuhuapi	5,079,598	687,575	16	8.1	7.5	3020	50.0	67.3	61.00	675.02	334.52	25.02
4	Puyuhuapi	5,079,607	687,621	21	9.1	7.5	3250	50.0	73.9	57.00	756.90	367.75	17.61
5	Ventisquero	5,084,056	693,183	12	5.0	6.8	2350	85.7	− 42.5	143.00	416.05	142.20	321.15
6	El Sauce	5,121,942	697,678	38	–	8.3	950	72.0	− 83.9	63.00	118.42	120.10	33.97
7	Isla Magdalena	5,062,248	681,263	5	16.3	7.1	4660	63.4	− 220.6	72.00	1349.61	219.47	17.86
8	Isla Magdalena	5,062,132	681,070	5	20.5	7.5	5340	77.1	− 225.2	75.00	1699.26	249.33	11.80
9	El Engaño	4,854,415	669,647	383	–	9.5	284	33.2	− 79.2	77.00	18.32	27.87	29.84
10	Huiña	4,868,685	667,620	276	–	7.9	217	39.3	202.6	50.00	10.16	17.03	47.47
11	Los Pobres	5,037,646	673,198	12	3.4	8.4	1308	47.7	− 105.6	54.00	280.57	191.29	32.58
12	Chilconal	4,979,824	649,828	51	4.7	7.2	2125	45.5	175.5	122.00	393.17	273.60	217.99
13	Puerto Peréz	4,988,243	641,401	7	8.6	6.9	1804	83.0	30.8	138.00	714.76	176.28	107.92
14	Puerto Cristal	4,835,765	697,255	212	–	8.0	872	54.1	− 137.0	59.00	137.72	50.52	129.19
15	Queulat	5,068,330	694,291	5	3.7	6.4	3000	37.4	56.4	131.00	310.03	136.71	1342.49
16	Río Rodriguez	5,144,136	683,911	18	–	9.3	445	61.4	− 173.5	59.00	61.81	43.98	21.25
20	Fiordo Puyuhuapi	5,084,720	692,506	3	F_jW	8.0	11,530	8.3	252.5	12.00	3540.69	485.02	35.15
21	Fiordo Pto. Cisne	5,038,584	673,625	0	F_jW	7.9	20,300	8.9	225.6	8.00	8283.97	1023.06	62.28
22	Fiordo de Aysén	4,980,789	648,663	0	F_jW	7.6	19,600	10.8	186.7	9.00	6869.31	926.90	58.70
30	Lluvia Bahia Murta	4,854,423	675,786	210	MW	5.9	62	7.4	141.5	0.14	1.24	0.24	2.03
31	Lluvia Coyhaique	4,854,423	675,786	304	MW	6.1	36	16.4	141.5	0.22	0.11	0.11	2.03
32	Lluvia Puyuhuapi	5,089,251	694,791	14	MW	6.0	198	8.1	195.2	0.01	0.26	< 0.05	1.53

Sample	CO_3^{2-}	Na^+	K^+	Ca^{2+}	Mg^{2+}	F^-	Br^-	Li	B	δD	δ18O	Balance
ID								[μg/l]		[‰(V-SMOW)]		[%]
1	–	1630.00	100.00	447.60	23.10	< 0.05	13.75	966.79	1216.33	− 51.47	− 7.71	− 2.92
2	1.02	64.00	2.90	1.71	0.14	0.47	0.13	10.33	302.17	− 58.33	− 9.58	5.57
3	–	366.00	13.76	172.80	1.05	0.50	2.68	17.75	448.75	− 59.46	− 7.56	− 2.90
4	–	402.00	12.96	189.90	0.89	0.51	2.97	18.59	472.31	− 64.10	− 7.73	− 3.51
5	–	336.00	27.80	61.00	2.95	1.17	1.56	525.28	656.72	− 67.84	− 8.66	− 3.69
6	1.38	133.00	3.45	9.88	0.02	1.37	0.50	38.15	362.44	− 61.53	− 8.24	− 1.19
7	–	528.00	20.55	320.50	1.62	0.16	5.71	106.78	137.00	− 53.21	− 8.18	− 4.10
8	–	624.00	23.15	380.50	4.04	0.15	7.20	124.82	166.95	− 53.54	− 8.35	− 6.33
9	3.19	51.60	1.84	2.69	0.01	3.96	0.07	44.37	56.16	− 89.22	− 12.28	12.14
10	–	33.40	0.79	5.13	0.18	7.02	< 0.05	54.88	47.19	− 87.12	− 11.83	− 1.26
11	–	212.00	9.40	26.94	6.74	0.62	1.13	100.27	157.92	− 59.39	− 9.33	− 4.68
12	–	334.00	31.00	72.15	4.37	0.71	1.47	1269.85	738.16	− 61.82	− 8.45	− 2.86
13	–	456.00	32.40	78.65	1.55	1.06	2.30	1635.36	4089.54	− 63.67	− 9.05	− 1.92
14	–	149.00	3.76	11.68	0.23	11.17	0.53	404.97	869.53	− 101.86	− 13.51	− 3.17
15	–	500.00	41.20	111.25	42.40	0.43	0.51	653.82	1951.78	− 62.67	− 7.79	− 2.72
16	0.71	76.50	1.97	3.19	0.01	0.29	0.28	61.36	526.72	− 59.74	− 8.47	7.41
20	–	1860.00	84.00	75.78	228.00	< 0.05	15.00	27.83	745.56	− 57.38	− 8.45	− 2.37
21	–	4460.00	194.50	168.20	518.00	< 0.05	34.84	61.63	1667.98	− 44.24	− 6.39	− 1.27
22	–	3330.00	158.50	138.00	424.00	< 0.05	26.86	52.14	1395.20	− 49.90	− 6.04	− 5.85
30	–	0.48	< 0.10	1.07	0.03	0.42	< 0.05	< 0.17	0.46	− 83.31	− 10.55	− 10.59
31	–	< 0.10	0.09	0.51	0.04	< 0.05	< 0.05	< 0.17	4.41	− 116.16	− 14.78	− 13.73
32	–	0.21	0.24	0.19	0.03	< 0.05	< 0.05	< 0.10	0.30	− 37.36	− 6.05	− 8.32

physico-chemical processes controlling the composition of water samples (Cloutier et al., 2008; Daniele et al., 2008; Güler et al., 2002; Tanasković et al., 2012). The statistical methods used in this study are hierarchical cluster analysis (HCA) and factorial analysis (FA).

HCA is a multivariate statistical technique that identifies relatively homogeneous clusters based on similarities of selected parameters. Samples with larger similarity are first grouped using a distance measure, subsequent samples are joined with a linkage rule until all samples have been classified. In this study, we used Euclidean distance and Ward's method, respectively. According to Güler et al. (2002), this combination produces the most distinctive geochemical clusters. Finally, HCA is visualized as a dendrogram, where the similarity between clusters is represented by the linkage distance at which the branches are connected.

FA is used to identify similarities and differences between variables and samples, helping on the data interpretation. This statistical method generated a small number of uncorrelated factors from a set of correlated variables that explain most of the variance without a substantial loss of information (Daniele et al., 2008). A subsequent geochemical interpretation for each factor will provide us an idea of the dominant hydrogeochemical processes that control the distribution of components in thermal waters. The number of extracted factors was determined using Kaiser's criterion, meaning that only factors with eigenvalues higher than one are retained. In addition, we applied the Bartlett and KMO (Kausir, Mayer and Olkin) test to assess the significance of the factorial model. A Varimax normalized rotation was used to maximize the variance and to facilitate the interpretation of the factors.

Sixteen thermal water samples, one fjord water and one meteoric water sample were used in the HCA and FA analysis. We choose the most saline fjord water sample and the most diluted meteoric water sample because they represent end-members of the geothermal fluid's recharge. The parameters used are T°, SiO_2, Cl^-, SO_4^{2-}, HCO_3^-, Na^+, Ca^{2+}, B, and Li. Concentration values lower than the detection limit were replaced by half of the detection limit value if they do not exceed 20% of the total data.

Most parameters show a high positive skewness and non-normal distribution. For this reason, they were log-transformed to approach a normal distribution, except for T° and SiO_2 whose distributions are close to normal. Afterward, the nine variables were normalized. Therefore, each variable has equal weight in the statistical analysis. Both data transformations are often used in multivariate statistical analysis (Cloutier et al., 2008; Güler et al., 2002).

3.3. Fjord water contribution

The chemical and isotopic composition of a binary mixing varies systematically depending on the relative abundance of their end member (Faure, 1998). Therefore, the fjord water contribution (f_s) was calculated as a theoretical percentage of a conservative mixing between meteoric water and fjord water considering: (1) Cl^- is a conservative element and (2) all Cl^- content has a fjord water origin (Daniele et al., 2013; Pulido-Leboeuf, 2004).

The fjord water contribution calculation considers Cl^- content in the geothermal water ($C_{Cl,sample}$), Cl^- concentration of the most diluted meteoric water ($C_{Cl,fw}$), and Cl^- content of the most saline fjord water sample ($C_{Cl,sw}$) as follows:

$$f_s = \frac{(C_{Cl,sample} - C_{Cl,fw})^*}{(C_{Cl,sw} - C_{Cl,fw})} 100$$

4. Results and discussion

4.1. Hydrogeochemical features and geochemical processes

The analytical measurements of the water samples are presented in Table 1. Thermal waters have a wide range of EC which varies from 217 μS/cm to 11,660 μS/cm. The samples with EC values above and below 1000 μS/cm correspond to thermal springs located in coastal (n° 1, 3, 4, 5, 7, 8, 11, 12, 13 and n° 15) and continental (n° 2, 6, 9, 10, 14 and n° 16) zones, respectively. Temperature ranges between 33.2 °C and 85.7 °C, the maximum temperature was measured in a shallow borehole (~40 m), located on the eastern shore of the Puyuhuapi fjord, 5 km south of the Puyuhuapi town (sample n° 5, Ventisquero, Table 1). The thermal waters pH ranges from 6.4 to 9.6, with higher values measured mostly in inland areas.

The Piper diagram shows different water types based on the ionic concentrations. Piper diagram (Fig. 2) indicates that Na^+ is the major cation, whereas Cl^- and HCO_3^- are the dominant anions in thermal springs. Thermal waters are mainly Na−Cl type and there are only two Na-HCO_3 water types. However, a curved hydrogeochemical evolution path is also distinguished from Ca-HCO_3 meteoric waters via Na-HCO_3 to Na−Cl thermal waters, suggesting that mixing and water-rock interaction processes can be driving the chemistry of the thermal springs samples (Appelo and Postma, 2004; Daniele et al., 2013; Srinivasamoorthy et al., 2011).

The concentrations of measured elements in thermal springs were plotted as a function of the measured temperatures show different trends (Fig. 3). These trends suggest that different hydrogeochemical processes are acting in these waters. Samples n° 1, 5, 12, 13 and n° 15 show greater concentrations of HCO_3^-, K^+, SiO_2, B and Li respect to others coastal thermal samples (Table 1 and Fig. 3) and will be differentiated with other colour to better display final results.

Ionic ratios versus chloride (Fig. 4) were plotted to evaluate the origin of dissolved components in the thermal waters if Cl^- is a conservative element. In the Br/Cl vs Cl^- scatter diagram (Fig. 4a) thermal springs fall close to fjord water values (1.5×10^{-3}) except for thermal spring n° 15 (7.3×10^{-4}), suggesting a fjord water contribution according to their geochemistry. This possibility is valid for thermal springs located in coastal zones, but it is surprising for inland thermal springs. Nevertheless, the Cl/Br ratios of Aysen inland samples (493 − 646) are in the range of values (300 − 650) reported by Alcalá and Custodio (2008) for inland areas with marine spray effects.

Another good tracer to identify the origin of soluble ions is the Na/Cl ratio. In fact, Na/Cl values greater or < 1.0 are related to non-marine or marine sources, respectively (Vengosh, 2003; Vengosh et al., 2002). In the Na/Cl vs Cl^- diagram (Fig. 4b) an increase in Na/Cl values is displayed for less saline waters. Na/Cl values greater than 1.5, related with non-marine (fjord, in this case) source, is the general trend of the inland thermal waters. Nevertheless, the sample n° 15, located in coastal zone, has a similar Na/Cl value (2.49) indicating a non-fjord source too, which is consistent with previously mentioned by Br/Cl ratio. Additionally, the samples n° 5, 11 and n° 12, located in coastal areas too, have Na/Cl values between 1.0 and 1.5, which could be interpreted that there is not a fjord water contribution. But, these increases in Na/Cl values can be explained by flushing of the mixing zone (Vengosh, 2003) or silicate weathering processes that contribute Na^+ ions to the hydrothermal system.

The same pattern is identified for the B/Cl, Li/Cl, SO_4/Cl and HCO_3/Cl ratios (Fig. 4c, d, e, f): An exponential decrease in the “ion/Cl” values at high chloride contents reaching values close to the fjord water samples. The high “ion/Cl” values, relative to fjord water ratio suggest that water-rock interaction processes and deep thermal solutions mixing could affect the geochemistry of Aysen thermal springs. Indeed, the high HCO_3/Cl and SO_4/Cl values respect to fjord water ratio in some thermal spring could suggest absorption of CO_2 and H_2S by volcanic degassing. Nevertheless, it cannot be discarded a contribution of

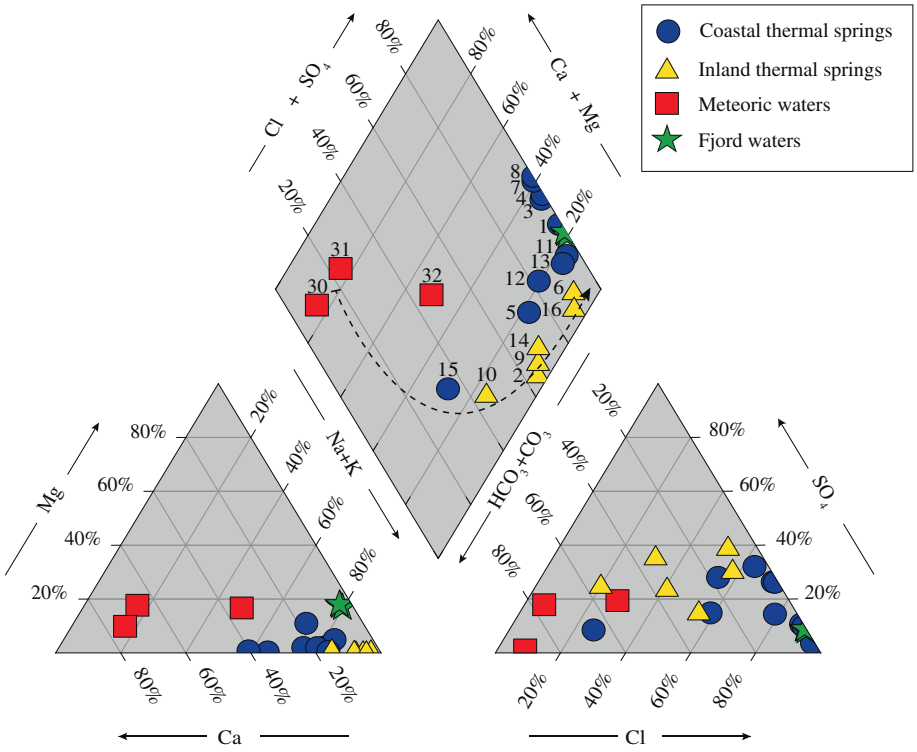

Fig. 2. Piper diagram of fjord, meteoric and thermal water samples.

HCO_3 from silicate weathering and dissolution of soil CO_2, and in case of SO_4 by sulphide oxidation. In addition, thermal springs with higher B/Cl and Li/Cl ratios than fjord water could indicate that rock dissolution processes are taken place. Both elements have significant concentration in igneous rock, being consistent with the host rock of the thermal springs (NPB). On the other hand, the 'ion/Cl' values close to fjord waters are usually observed in coastal thermal springs (except the sample n° 15) where fjord water mixing is probably the dominant process in the geochemistry of these thermal waters.

In the Fig. 5 is shown the variation of the B/Cl and Br/Cl ratios, proposed by Vengosh (2003) to differentiates between multiple salinity sources. The thermal springs fall in two domains linked to hydrothermal and marine sources, which coincide with previously proposed sources. In fact, the dominant process for thermal springs n° 7 and n° 8 (Isla Magdalena area) is seawater intrusion (Fig. 5), being consistent with depletion in the Na/Cl values and excesses in the SO_4/Cl and Ca/Cl values respect to fjord waters (Fig. 4) interpreted as actual fjord water intrusion in the system (Daniele et al., 2013).

4.2. Saline factor

As there is not a relationship between temperature and chloride content (Fig. 3), δ^2H and $\delta^{18}O$ don't show a significant influence of volcanic fluids (Fig. 9) and no other chloride sources different to fjord were distinguished in coastal thermal fluids except for thermal spring n° 15 (Fig. 4a), so it can be assumed that all chlorine in these samples has a fjord origin. Therefore, the saline factor can be calculated as fjord water percentage.

The fjord water percentages calculated is shown in Table 1. The highest fjord water percentage is 42.3% for thermal spring n° 1. This springs outflow at fjord water table elevation and it is visible only with low tide. High fjord water percentages were also calculated for the samples n° 3, 4, 7 and n° 8, indicating that fjord water mixing is an important process in the chemistry of these thermal waters. The differences observed in SiO_2, HCO_3^-, Ca^{2+}, F^-, Li and B could be related to the not conservative chemical behavior of these elements. Samples without a calculated saline factor are inland thermal springs with no influence of fjord water.

4.3. Water-rock interaction processes

Different chemical reactions such as dissolution/precipitation, oxidation/reduction and ion exchange processes can influence in the chemistry of waters during water-rock interaction processes where carbonate-silicate weathering, halite-gypsum dissolution and precipitation are common in groundwater systems (Elango and Kannan, 2007). In addition, almost all ions except for bromide suggest that water-rock interaction processes exert an influence on the thermal waters (Fig. 4), mainly in inland areas, where it is probably a dominant process that controls the chemistry of these samples.

In the (Ca + Mg) vs. (HCO_3 + SO_4) diagram (Fig. 6a) most thermal waters plot below the 1:1 ratio line, suggesting that silicate weathering is taking place, which is consistent with the mineralogy of the host rock (NPB). In addition, higher SiO_2 concentration relative to fjord and meteoric water samples, Na/Cl ratios > 1.0 and (Na + K) excess over Cl^-, support the hypothesis of a chemical component contribution via silicate weathering (Srinivasamoorthy et al., 2011; Stallard and Edmond, 1983). On the other hand, Fig. 6a shows an increase in (Ca + Mg) contents without variations in (HCO_3 + SO_4) in the samples n° 1, 3, 4, 7, and n°8. These thermal springs have the highest fjord water contribution (Table 1), and therefore, the increase in (Ca + Mg) contents may be due to XNa^+-1/2XCa^{+2} cation exchange in the saltwater wedge, an important and common process in the chemistry of coastal aquifers (Appelo and Postma, 2004). Moreover, most of the thermal waters plot along the line with a slope of −1 in the (Ca + Mg-HCO_3-SO_4) vs. (Na + K-Cl) scatter diagram (Fig. 6b), suggesting that cation exchange is a significant process in thermal springs (Fisher and Mullican, 1997; Kim et al., 2004). However, the samples n° 1, 3, 4, 7 and n° 8 are not in line with this relationship, probably indicating that fjord water mixing is the dominant process in these thermal springs. In addition, inland thermal springs also plot along the line with a slope of −1, probably because Ca^{2+} is being controlled by cation exchange

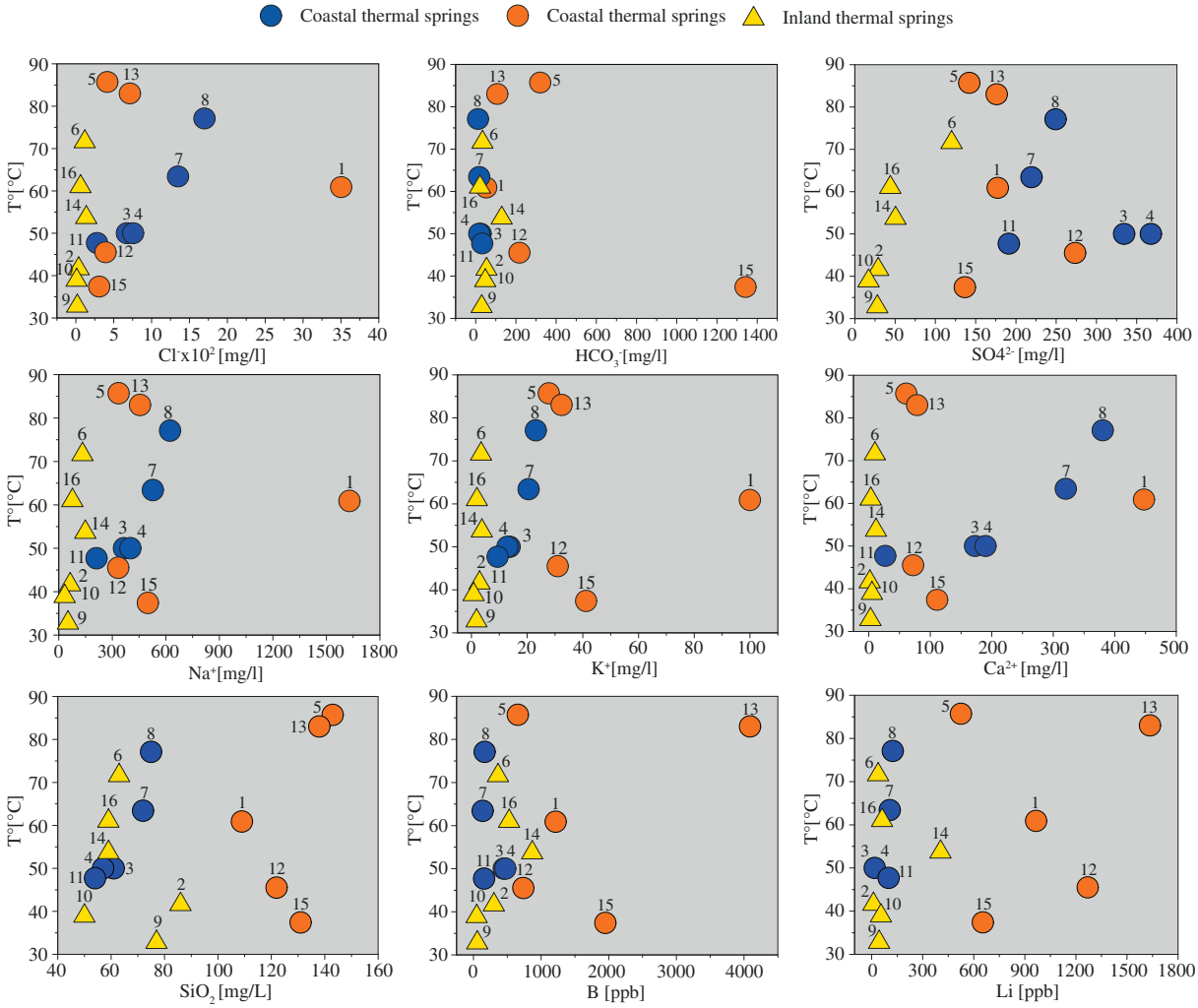

Fig. 3. Dissolved ions [mg/l] vs. surface temperatures [°C] of thermal water samples. Different colours in coastal thermal springs are to better display final results. (For interpretation of the references to colour in this figure legend, the reader is referred to the web version of this article.)

with Na^+ in silicate minerals such as clays and zeolites, instead of dissolution of carbonate (Fournier and Truesdell, 1973).

4.4. Multivariate statistical analysis

HCA is shown as a dendrogram (Fig. 7). A segmented horizontal line was drawn across the dendrogram "*phenon line*" at a linkage distance of five (Fig. 7). Thus, water samples below the *phenon line* were grouped into the same cluster. We identify three main clusters (G1, G2 and G3) and one isolated water sample of meteoric water. The cluster G1 includes thermal waters located on the coastline (coastal thermal waters symbolized with blue colour) and the fjord water sample. These samples are Na−Cl type water with the highest average concentrations of Cl^--SO_4^{2-}-Na^+-Ca^{2+} (Table 2). The cluster G2 only includes thermal springs located inland, and they are mainly Na-Cl-HCO_3 water type, showing a geochemical trend from Na-HCO_3 to Na−Cl water type (Fig.2). These samples have higher average values of T°, SiO_2, HCO_3^- and Li than G1 (Table 2). Finally, the cluster G3 includes thermal springs located on the coastline (coastal thermal waters symbolized with orange colour) with the highest average values of T°-SiO_2-HCO_3^--Li-B (Table 2). These samples are mainly Na−Cl water type and show a geochemical trend from Na-HCO_3 to Na−Cl water type (Fig.2).

On the other hand, Fig. 7 shows dissimilarities among clusters. G1 and G2 relate to the lowest linkage distance (around 6), indicating a higher affinity. Then, both clusters join with G3 at a higher linkage distance (8), suggesting a lower chemical affinity with the mixture of G1 and G2. On the other hand, the meteoric water sample is linked at a high linkage distance (nearly 12), indicating that it is not enough by itself to generate the chemical composition of the other clusters.

Factorial analysis of the hydrogeochemical dataset is shown in Table 3. Two loading factors were identified with eigenvalues greater than one, accounting for 82.1% of the total dataset variance. The weight of the variables in each factor are called "loading" and each factor is associated with at least one variable. Loading values > 0.5 are marked in bold, which represent the importance of that variable for the factor (Table 3).

Factor 1 accounts for most of the dataset variance (66.4%), and is correlated with Cl^-, $SO4^{2-}$, Na^+, Ca^{2+}, Li and B (Table 3). These variables are found in large concentration in fjord water samples and therefore we interpreted them as indicator of fjord water mixing processes. Factor 2 (15.7%) is determined by positive loading in T°, SiO_2, HCO_3^-, Li and B (Table 3). This is consistent with silicate weathering at high temperature incorporating SiO_2, Li and B to the fluid (Ellis and Mahon, 1964, 1967, 1977). Nevertheless, at high temperatures, B and HCO_3 can be transported as H_3BO_3 and CO_2 (Giggenbach, 1991), so a volcanic degassing contribution cannot be discarded. These two processes will be grouped and named as "magmatic-hydrothermal" input of fluids. In addition, boron and lithium have significant loading values in both factors (Table 3), which we interpret as two different sources. Nevertheless, lithium has a higher loading value in factor 2, suggesting

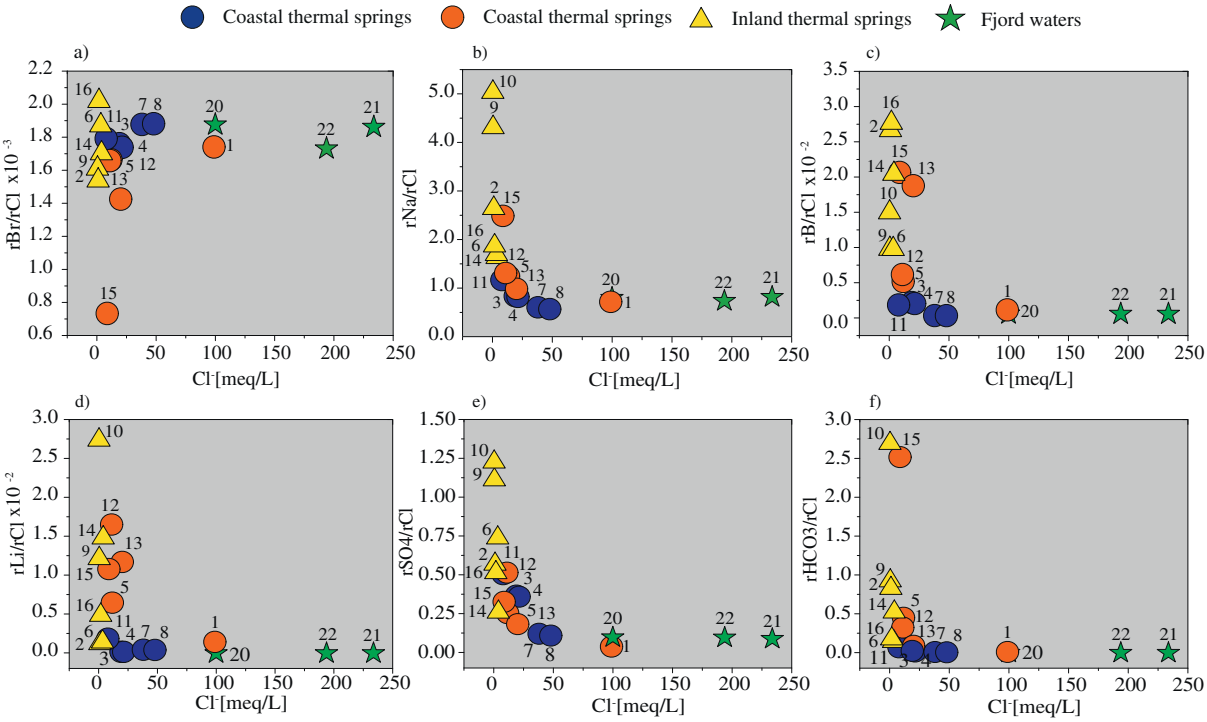

Fig. 4. rBr/rCl, rNa/rCl, rB/rCl, rLi/rCl, rSO_4/rCl, $rHCO_3$/rCl ratios vs. Cl^-[meq/l] in thermal and fjord water sample (r means that concentration is in meq/L).

a higher contribution from silicate weathering at high temperature. These interpretations are coherent with fjord water and hydrothermal sources identified in Fig. 5.

The factorial scores obtained from the FA (Fig. 8) show the same clusters (G1 − G3) as indicated by the HCA (Fig. 7). However, the most relevant hydrogeochemical processes controlling the chemistry of thermal springs are also identified for each cluster. G1 is mainly influenced by fjord water mixing. G2 is related to an input of magmatic-hydrothermal fluids, yet springs n° 9 and n° 10 show a negative factor 2, suggesting they are probably influenced only by dissolution and precipitation processes, without a magmatic-hydrothermal component. G3 shows a very positive factor 2, suggesting a dominance of magmatic-hydrothermal components with little influence of fjord water mixing, except for thermal spring n° 1, which has a strong fjord component (42.3% of saline factor; Table 1). In addition, G3 shows a stronger influence of factor 2 than G2, which correlates to higher temperatures measured in some thermal springs (n° 1, 5 and n° 13), probably causing higher rates of rock dissolution and/or input of magmatic fluids.

4.5. Isotope composition

The stable isotopic composition of δ^2H and $\delta^{18}O$ in thermal springs plots along the local meteoric water line (LMWL) and global meteoric water line (GMWL), showing a clear relationship with actual meteoric waters, as shown in Fig. 9. However, δ^2H and $\delta^{18}O$ data could not show a clear isotopic shift respect to LMWL even when up to 10% of fluids composition have a different source (Nicholson, 1993). That means that a magmatic contribution diluted with meteoric water cannot be discarded. In fact, the Aysen thermal springs show small δ^2H and/or $\delta^{18}O$ deviations, in both directions, from the LMWL (Fig. 9). Left shifts have

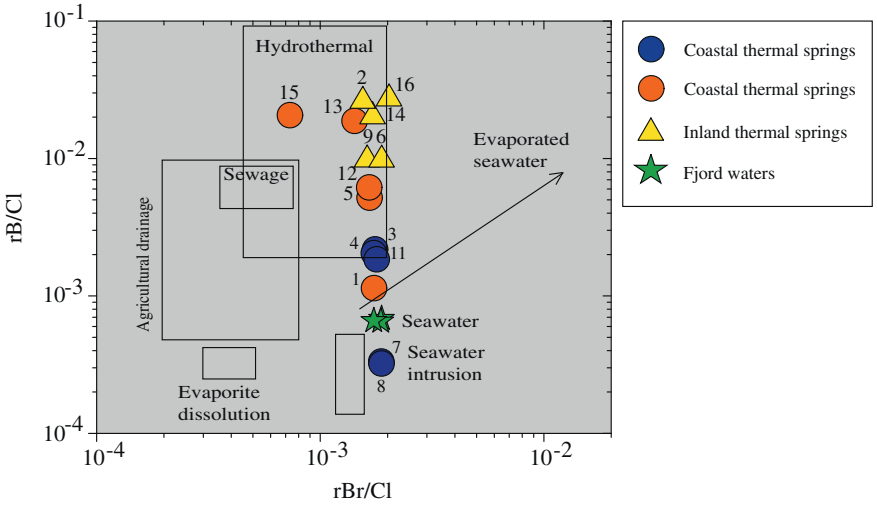

Fig. 5. rB/rCl vs. rBr/rCl binary diagram (Vengosh, 2003) in thermal and fjord water samples (r means that concentration is in meq/L).

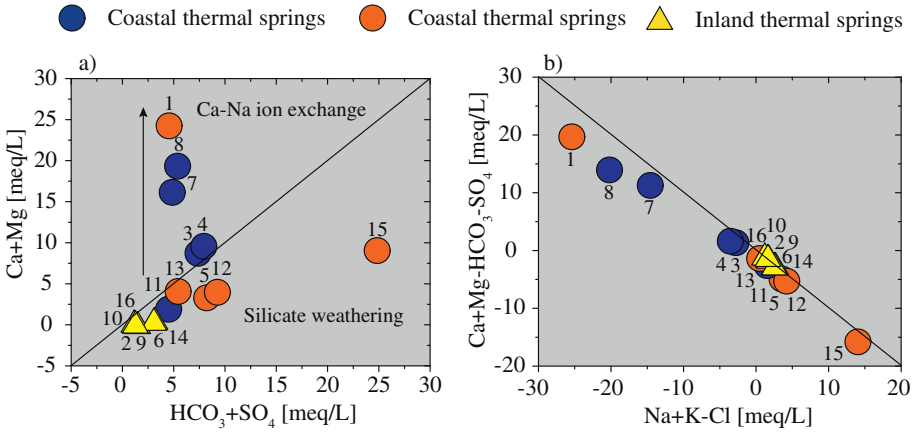

Fig. 6. Ca + Mg-HCO_3-SO_4 vs. Na + K-Cl and Ca + Mg vs. HCO_3 + SO_4 binary diagrams showing different water-rock interaction processes.

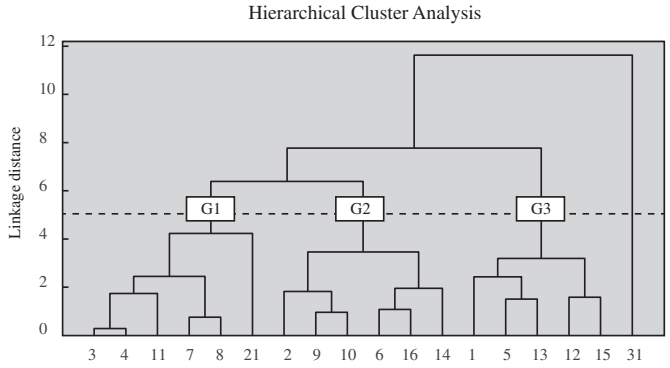

Fig. 7. Dendogram from the HCA for water samples. Segmented line defines "phenon line" at a linkage distance of five.

been usually associated with H_2S and CO_2 exchange, hydration of silicates and low temperature minerals reaction. Instead, right shifts have been interpreted as CO_2 exchange, high temperature exchange minerals (above 250 °C), evaporation from surface and mixing with marine waters (Karolyte et al., 2017). Even if we cannot differentiate which of the above processes are acting in each sample, we suggest, according with our data interpretation that fjord water mixing, mineral reaction and CO_2 exchange could induce these small deviations.

Regardless two groups with clear differences in δ^2H and $\delta^{18}O$ are distinguished in the Fig. 9. This variation is probably related to a continental effect (Giggenbach, 1991), causing depletion in heavier isotopes for the recharge water of the thermal springs located in the eastern side of the Andean mountain range (n° 9, 10 and n° 14) (Fig. 1). Those isotopic signatures are consistent with the meteoric water sampled in surrounding areas (n° 31). This suggests different recharge sources for the thermal springs, which are derived from isotopically different meteoric water.

Table 3
Factorial analysis with Varimax rotation. Bold value corresponds to significant variables in each factor.

Factor Loading with Varimax normalized rotation		
Parameters	Factor 1	Factor 2
T°	0.22	**0.58**
SiO2	0.13	**0.93**
HCO3	0.22	**0.83**
Cl	**0.96**	0.25
SO4	**0.93**	0.28
Na	**0.91**	0.36
Ca	**0.88**	0.19
Li	**0.51**	**0.79**
B	**0.64**	**0.62**
Eigenvalor	5.98	1.41
Explained variance (%)	66.4	15.7
Cumulative % of variance	66.4	82.1

4.6. Geothermometers

Geothermometers are empirical equations commonly used to estimate the subsurface temperature of thermal fluids. They are based on the temperature dependence equilibrium between specific mineral or mineral assemblage and solution during water-rock interaction processes taking place in a geothermal reservoir. For this reason, any change in the chemical constituents of fluids equilibrium conditions (i.e., dilution, boiling, mixing, mineral precipitation and re-equilibration among others) during their ascent to the surface could result in biased temperatures (Fournier, 1977; Nicholson, 1993).

The estimated subsurface temperature of thermal springs is highly variable and depends on the used geothermometers (Table 4). Silica geothermometers (Fournier, 1977; Fournier and Potter, 1982) predict a temperature ranging from 102 to 158 °C (Table 4). Lower temperatures were generally obtained in inland thermal springs, although coastal

Table 2
Average values and standard deviation for G1, G2 and G3 water groups distinguished in the HCA.

Group	Number of water samples	T°	SiO2	Cl-	SO4-2	HCO3 −	Na +	Ca + 2	Li	B
		[°C]	[mg/l]						[ppb]	
G1	6	49.5	54.5	2174.2	397.6	27.9	1098.7	209.8	71.6	508.5
	(3, 4, 7, 8, 11, 21)	(± 22.8)	(± 24.2)	(± 3035.7)	(± 313.8)	(± 18.3)	(± 1652.7)	(± 125.2)	(± 46.3)	(± 587.7)
G2	6	50.3	65.7	63.9	48.1	52.6	84.6	5.7	102.3	360.7
	(2, 6, 9, 10, 14, 16)	(± 14.8)	(± 13.3)	(± 53.2)	(± 37.3)	(± 39.4)	(± 46.2)	(± 4.1)	(± 149.3)	(± 310.1)
G3	5	62.5	128.6	1067.7	181.3	408.5	651.2	154.1	1010.2	1730.5
	(1, 5, 12, 13, 15)	(± 21.7)	(± 13.5)	(± 1370.7)	(± 54.9)	(± 532.2)	(± 552.0)	(± 165.1)	(± 453.4)	(± 1415.6)

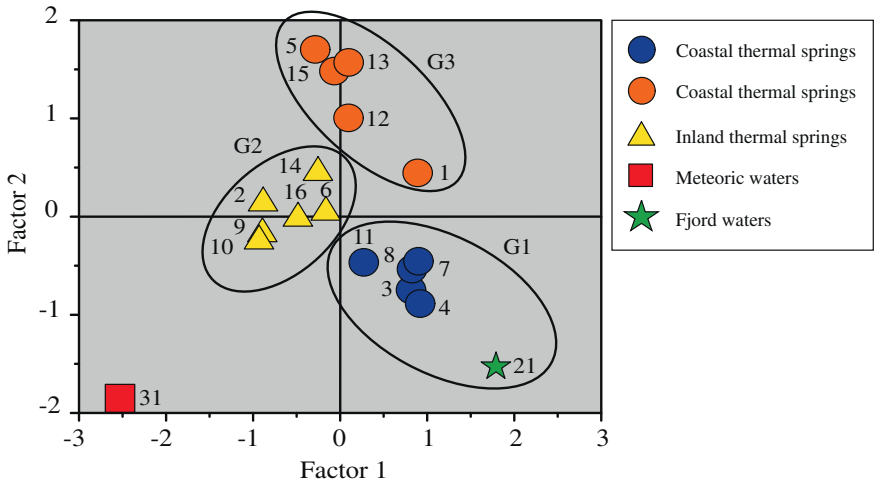

Fig. 8. Plot of factorial scores. The HCA groups are shown.

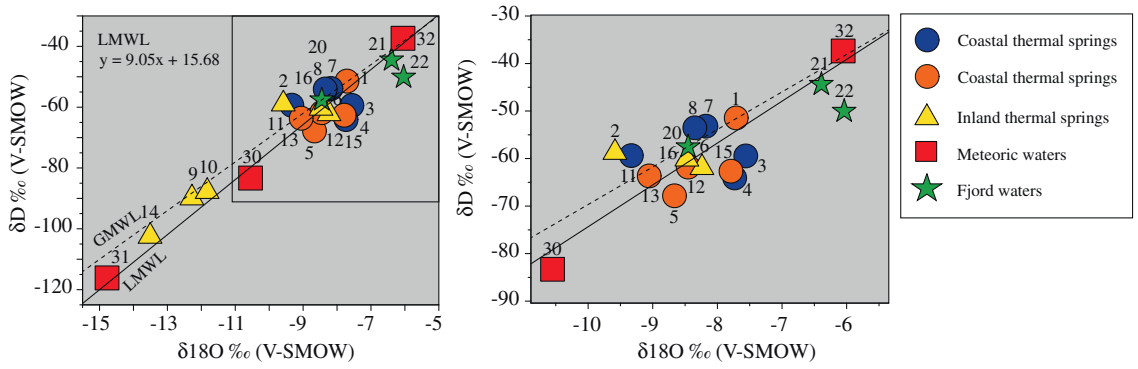

Fig. 9. Binary graph δ^2H vs. $\delta^{18}O$ for water samples taken. GMWL: global meteoric water line (Craig, 1963); LMWL: local meteoric water line.

Table 4
Estimated reservoir temperature by silica and cations geothermometers.

Sample ID	Geothermometers						
	Quartz[a]	Quartz[a] (steam loss)	Quartz[b]	Na/K[c]	Na/K[d]	Na/K[e]	Na/K[f]
1	142	137	142	196	178	141	170
2	129	126	129	176	157	116	143
3	111	111	112	165	145	102	127
4	108	108	108	156	136	91	116
5	158	150	158	218	201	168	201
6	113	112	113	144	123	77	100
7	120	118	120	167	148	104	130
8	122	120	122	164	145	101	126
9	123	121	123	162	142	98	123
10	102	103	102	139	118	72	94
11	106	106	106	175	156	114	141
12	149	142	149	226	211	180	214
13	156	149	156	206	189	154	185
14	110	109	110	142	122	75	98
15	153	146	153	217	201	168	201
16	110	109	110	143	123	77	99

[a] Fournier (1977).
[b] Fournier and Potter (1982).
[c] Giggenbach (1988).
[d] Fournier (1979).
[e] Truesdell and Fournier (1975).
[f] Tonani (1980).

thermal springs are mixed with fjord water decreasing the silica contents, and therefore the estimated reservoir temperatures. Furthermore, we calculated the saturation index for quartz in all thermal springs giving results greater than zero. This led to a decrease of the silica content in thermal fluids by precipitation of quartz during their ascent, estimating lower reservoir temperatures.

The Na/1000-K/100-$Mg^{0.5}$ ternary plot proposed by Giggenbach (1988) shows that the thermal springs fall in immature and partial equilibrium/mixing fields (Fig. 10). This suggests that the equilibrium conditions of the thermal springs have not been reached, probably due to limited water-rock interaction and/or mixing processes. In fact, the fjord water contribution is one of the factors that alter the calculated temperatures of cationic geothermometers (Dotsika, 2015; Dotsika et al., 2010). Thus, the estimated temperatures can only be considered tentative, especially in coastal thermal springs.

Na–K geothermometers (Fournier, 1979; Giggenbach, 1988; Tonani, 1980; Truesdell and Fournier, 1975) indicate reservoir temperatures from 72 to 226 °C for Aysen thermal springs (Table 4). Lower temperatures were also estimated in inland thermal springs with temperatures ranged between 72 and 176 °C. Nonetheless, temperatures lower than 180 °C using Na–K geothermometers might give wrong results (Arnórsson et al., 1983b), and therefore should be treated with caution.

5. Conclusions

The physico-chemical data of Aysen thermal springs was analysed

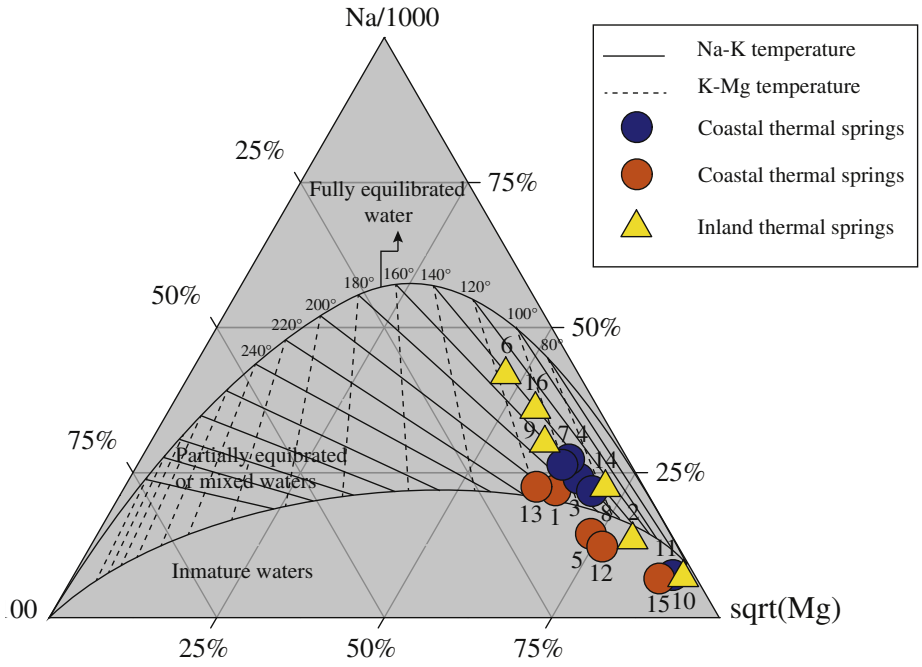

Fig. 10. Ternary diagram of Aysen thermal springs based on Na/1000-K/100-$Mg^{0.5}$ (Giggenbach, 1988).

using classic geochemical tools and multivariate statistical analysis (HCA and FA). The results indicate three groups of thermal springs and two dominant hydrogeochemical processes. G1 located along the coastline is mainly controlled by fjord water mixing. G2 located in inland areas shows an input of magmatic-hydrothermal fluids, except for the thermal springs n° 9 and n° 10, which are probably influenced only by dissolution/precipitation processes. G3 includes samples located in coastal areas which seem to be dominated by input of magmatic-hydrothermal fluids with a lower influence of fjord water mixing, except for thermal spring n° 1, which has a strong fjord component (42.3% of saline factor). In addition, this group presents the highest estimated reservoir temperatures, which increase the rate of rock dissolution. On the other hand, the saline factor of all coastal samples ranges from 3.4% to 42.3%, supporting the hypothesis that fjord water mixing is a dominant process. In addition, silicate weathering and XNa^+-1/$2XCa^{2+}$ ion exchange are significant water-rock interaction processes, also controlling the chemical composition of thermal fluids.

The stable isotopic composition of δ^2H and $\delta^{18}O$ in thermal spring plots along the LMWL, showing a clear source from meteoric waters, without an important contribution from magmatic sources, suggesting a short residence time of recharge waters, and a limited isotopic exchange during water-rock interaction processes. Small deviations in $\delta^{18}O$ values have been interpreted as fjord water mixing, dissolution/precipitation and CO_2 exchange processes.

Acknowledgements

The authors acknowledge the support of CONICYT FONDAP Project n° 15090013 (Andean Geothermal Center of Excellence, CEGA), project FONDEQUIP EQM120098, Gobierno Regional Aysen geothermal project Code BIP 30346723-0 and Stable Isotope Laboratory (Instituto Andaluz de Ciencias de la Tierra, CSIC-Univ. Granada) in funding this research. We are grateful to Veronica Rodriguez, who performs the water chemical analysis. The authors wish to acknowledge the three anonymous reviewers for helpful suggestions which certainly led to an overall improvement of the manuscript. We appreciate the collaboration of thermal spas that allow us the samples collection.

References

Alam, M.A., Sánchez, P., Parada, M.A., 2010. Interplay of volcanism and structural control in defining the geothermal system (s) along the Liquiñe-ofqui Fault Zone, in the south-central Chile. gRC Trans. 34, 747–750.
Alcalá, F.J., Custodio, E., 2008. Using the Cl/Br ratio as a tracer to identify the origin of salinity in aquifers in Spain and Portugal. J. Hydrol. 359, 189–207.
Appelo, C.A.J., Postma, D., 2004. Geochemistry, Groundwater and Pollution. CRC Press, Second Edition.
Arancibia, G., Cembrano, J., Lavenu, A., 1999. Transpresión dextral y partición de la deformación en la Zona de Falla Liquiñe-Ofqui, Aisén, Chile (44-45°S). Rev. Geol. Chile 26, 3–22.
Aravena, D., Muñoz, M., Morata, D., Lahsen, A., Parada, M.Á., Dobson, P., 2016. Assessment of high enthalpy geothermal resources and promising areas of Chile. Geothermics 59, 1–13.
Arnórsson, S., Gunnlaugsson, E., Svavarsson, H., 1983a. The chemistry of geothermal waters in Iceland. II. Mineral equilibria and independent variables controlling water compositions. Geochim. Cosmochim. Acta 47, 547–566.
Arnórsson, S., Gunnlaugsson, E., Svavarsson, H., 1983b. The chemistry of geothermal waters in Iceland. III. Chemical geothermometry in geothermal investigations. Geochim. Cosmochim. Acta 47, 567–577.
Benavente, O., Tassi, F., Gutiérrez, F., Vaselli, O., Aguilera, F., Reich, M., 2013. Origin of fumarolic fluids from Tupungatito Volcano (Central Chile): interplay between magmatic, hydrothermal, and shallow meteoric sources. Bull. Volcanol. 75, 1–15.
Benavente, O., Tassi, F., Reich, M., Aguilera, F., Capecchiacci, F., Gutiérrez, F., Vaselli, O., Rizzo, A., 2016. Chemical and isotopic features of cold and thermal fluids discharged in the Southern Volcanic Zone between 32.5° S and 36° S: insights into the physical and chemical processes controlling fluid geochemistry in geothermal systems of Central Chile. Chem. Geol. 420, 97–113.
Bertrand, S., Hughen, K.A., Sepulveda, J., Pantoja, S., 2012. Geochemistry of surface sediments from the fjords of Northern Chilean Patagonia (44 – 47°S): spatial variability and implications for paleoclimate reconstructions. Geochim. Cosmochim. Acta 76, 125–146.
Capaccioni, B., Aguilera, F., Tassi, F., Darrah, T., Poreda, R.J., Vaselli, O., 2011. Geochemical and isotopic evidences of magmatic inputs in the hydrothermal reservoir feeding the fumarolic discharges of Tacora volcano (northern Chile). J. Volcanol. Geotherm. Res. 208, 77–85.
Cembrano, J., Hervé, F., 1993. The Liquine Ofqui Fault Zone: a major Cenozoic strike slip duplex in the southern Andes. In: Second ISAG. Oxford, pp. 175–178.
Cembrano, J., Lara, L., 2009. The link between volcanism and tectonics in the southern volcanic zone of the Chilean Andes: a review. Tectonophysics 471, 96–113.
Cembrano, J., Hervé, F., Lavenu, A., 1996. The Liquine Ofqui fault zone: a long-lived intra-arc fault system in southern Chile. Tectonophysics 259, 55–66.
Cembrano, J., Lavenu, A., Reynolds, P., Arancibia, G., López, G., Sanhueza, A., 2002. Late Cenozoic transpressional ductile deformation north of the Nazca – South America – Antarctica triple junction. Tectonophysics 354, 289–314.
Cloutier, V., Lefebvre, R., Therrien, R., Savard, M.M., 2008. Multivariate statistical analysis of geochemical data as indicative of the hydrogeochemical evolution of groundwater in a sedimentary rock aquifer system. J. Hydrol. 353, 294–313.
Coleman, M.L., Shepherd, T.J., Durham, J.J., Rouse, J.E., Moore, G.R., 1982. Reduction of

water with zinc for hydrogen isotope analysis. Anal. Chem. 54, 993–995.
Cortecci, G., Boschetti, T., Mussi, M., Lameli, C.H., Mucchino, C., Barbieri, M., 2005. New chemical and original isotopic data on waters from El Tatio geothermal field, northern Chile. Geochem. J. 39, 547–571.
Craig, H., 1963. The isotopic geochemistry of water and carbon in geothermal areas. Nucl. Geol. Geotherm. Areas 17–53.
Daniele, L., Bosch, A.P., Vallejos, A., Molina, L., 2008. Geostatistical analysis to identify hydrogeochemical processes in complex aquifers: a case study (Aguadulce unit, Almeria, SE Spain). AMBIO A J. Hum. Environ. 37, 249–253.
Daniele, L., Vallejos, Á., Corbella, M., Molina, L., Pulido-Bosch, A., 2013. Hydrogeochemistry and geochemical simulations to assess water-rock interactions in complex carbonate aquifers: the case of Aguadulce (SE Spain). Appl. Geochemistry 29, 43–54.
De la Cruz, R., Suárez, M., 2006. Geología del área Puerto Guadal-Puerto Sánchez: Región Aisén del General Carlos Ibáñez del Campo. (Servicio Nacional de Geología y Minería).
D'Orazio, M., Innocenti, F., Manetti, P., Tamponi, M., Tonarini, S., González-Ferrán, O., Lahsen, A., Omarini, R., 2003. The Quaternary calc-alkaline volcanism of the Patagonian Andes close to the Chile triple junction: geochemistry and petrogenesis of volcanic rocks from the Cay and Maca volcanoes (~45°S, Chile). J. S. Am. Earth Sci. 16, 219–242.
Dotsika, E., 2015. H-O-C-S isotope and geochemical assessment of the geothermal area of Central Greece. J. Geochem. Explor. 150, 1–15.
Dotsika, E., Poutoukis, D., Raco, B., 2010. Fluid geochemistry of the Methana peninsula and Loutraki geothermal area, Greece. J. Geochemical Explor. 104, 97–104.
Duriez, A., Marlin, C., Dotsika, E., Massault, M., Noret, A., Morel, J.L., 2008. Geochemical evidence of seawater intrusion into a coastal geothermal field of central Greece: example of the Thermopylae system. Environ. Geol. 54, 551–564.
Elango, L., Kannan, R., 2007. Rock-water interaction and its control on chemical composition of groundwater. Dev. Environ. Sci. 5, 229–243.
Ellis, A.J., Mahon, W.A.J., 1964. Natural hydrothermal systems and experimental hot-water/rock interactions. Geochim. Cosmochim. Acta 28, 1323–1357.
Ellis, A.J., Mahon, W.A.J., 1967. Natural hydrothermal systems and experimental hot water/rock interactions (part II). Geochim. Cosmochim. Acta 31, 519–538.
Ellis, A.J., Mahon, W.A.J., 1977. Chemistry and Geothermal Systems. Academic Press, New York.
Epstein, S., Mayeda, T., 1953. Variation of the O18/O16 ratio in natural waters. Geochim. Cosmochim. Acta 4, 213–224.
Fang, Z., Boucot, A., Covacevich, V., Herve, F., 1998. Discovery of late Triassic fossils in the Chonos metamorphic complex, southern Chile. Rev. Geol. Chile 25, 165–173.
Faure, G., 1998. Principles and Applications of Geochemistry: A Comprehensive Textbook for Geology Students. (Prentice Hall).
Fisher, R.S., Mullican III, W.F., 1997. Hydrochemical evolution of sodium-sulfate and sodium-chloride groundwater beneath the northern Chihuahuan Desert, trans-Pecos, Texas, USA. Hydrogeol. J. 5, 4–16.
Fournier, R.O., 1977. Chemical geothermometers and mixing models for geothermal systems. Geothermics 5, 41–50.
Fournier, R.O., 1979. A revised equation for the Na/K geothermometer. Geotherm. Resour. Counc. Trans. 3, 221–224.
Fournier, R.O., Potter, R.W., 1982. Revised and expanded silica (quartz) geothermometer. Bull., Geotherm. Resour. Counc. (Davis, Calif.); (United States) 11.
Fournier, R.O., Truesdell, A.H., 1973. An empirical Na-K-Ca geothermometer for natural waters. Geochim. Cosmochim. Acta 37, 1255–1275.
Giggenbach, W.F., 1988. Geothermal solute equilibria. Derivation of Na-K-Mg-Ca geoindicators. Geochim. Cosmochim. Acta 52, 2749–2765.
Giggenbach, W.F., 1991. Isotopic composition of geothermal water and steam discharges. Appl. Geochemistry Geotherm. Reserv. Dev. 253–273.
Giggenbach, W.F., 1995. Variations in the chemical and isotopic composition of fluids discharged from the Taupo Volcanic Zone, New Zealand. J. Volcanol. Geotherm. Res. 68, 89–116.
Giggenbach, W.F., Goguel, R.L., 1989. Collection and analysis of geothermal and volcanic water and gas discharge. In: Department of Scientefic and Industrial Research, Chemistry Division, pp. 1989.
Güler, C., Thyne, G.D., McCray, J.E., Turner, K.A., 2002. Evaluation of graphical and multivariate statistical methods for classification of water chemistry data. Hydrogeol. J. 46, 763–774.
Gutiérrez, F., Gioncada, A., Ferran, O.G., Lahsen, A., Mazzuoli, R., 2005. The Hudson Volcano and surrounding monogenetic centres (Chilean Patagonia): an example of volcanism associated with ridge-trench collision environment. J. Volcanol. Geotherm. Res. 145, 207–233.
Hauser, A., 1989. Thermal and Mineral Springs around the southern highway, regions X – XI, Chile. Rev. Geol. Chile 16, 229–239.
Hauser, A., 1997. Catastro y caracterización de las fuentes de aguas minerales y termales de Chile. Servicio Nacional de Geología y Minería. Santiago, Chile.
Herve, F., Fanning, C.M., 2001. Late Triassic detrital zircons in meta-turbidites of the Chonos Metamorphic Complex, southern Chile. Rev. Geol. Chile 28, 91–104.
Herve, F., Mpodozis, C., Davidson, J., Godoy, E., 1981. Observaciones estructurales y petrográficas en el basamento metamórfico del archipiélago de Los Chonos, entre el canal King y el canal Ninualac. Aisén. Rev. Geol. Chile 13 – 14, 3–16.
Hervé, F., Godoy, E., Garrido, I., Hormazábal, L., Brook, M., Pankhurst, R.J., Vogel, S., 1988. Geocronologia y condiciones de metamorfismo del complejo de subduccion del archipielago de los Chonos. Congreso Geológico Chileno 5.
Herve, F., Fanning, C.M., Pankhurst, R.J., 2003. Detrital zircon age patterns and provenance of the metamorphic complexes of southern Chile. J. S. Am. Earth Sci. 16, 107–123.
Hervé, F., Calderón, M., Faúndez, V., 2008. The metamorphic complexes of the Patagonian and Fuegian Andes. Geol. Acta 6, 43–53.
Hervei, F., Pankhurst, R.J., Drake, R., Beck, M.E., 1995. Pillow metabasalts in a mid-Tertiary extensional basin adjacent to the Liquiñe-Ofqui fault zone: the Isla Magdalena area, Aysen, Chile. J. S. Am. Earth Sci. 8, 33–46.
Karolyte, R., Serno, S., Johnson, G., Gilfillan, S.M.V., 2017. The influence of oxygen isotope exchange between CO_2 and H_2O in natural CO_2-rich spring waters: implications for geothermometry. Appl. Geochemistry 84, 173–186.
Kim, K., Rajmohan, N., Kim, H.J., Hwang, G.-S., Cho, M.J., 2004. Assessment of groundwater chemistry in a coastal region (Kunsan, Korea) having complex contaminant sources: a stoichiometric approach. Environ. Geol. 46, 763–774.
Lagabrielle, Y., Suárez, M., Rossello, E.A., Hérail, G., Martinod, J., Régnier, M., De la Cruz, R., 2004. Neogene to Quaternary tectonic evolution of the Patagonian Andes at the latitude of the Chile Triple Junction. Tectonophysics 385, 211–241.
Lahsen, A., López Escobar, L., Vergara, M., 1994. The Puyuhuapi volcanic group, Southern Andes (44°20′S): geological and geochemical antecedents. In: 7 Congreso Geológico Chileno. 11. Chile, Concepción, pp. 1076–1079.
Legrand, D., Barrientos, S., Bataille, K., Cembrano, J., Pavez, A., 2011. The fluid-driven tectonic swarm of Aysen Fjord, Chile (2007) associated with two earthquakes (Mw = 6.1 and Mw = 6.2) within the Liquiñe-Ofqui Fault Zone. Cont. Shelf Res. 31, 154–161.
Millot, R., Hegan, A., Négrel, P., 2012. Geothermal waters from the Taupo Volcanic Zone, New Zealand: Li, B and Sr isotopes characterization. Appl. Geochemistry 27, 677–688.
Nicholson, K., 1993. Geothermal Fluids : Chemistry and Exploration Techniques. Springer Berlin Heidelberg, Berlin, Heidelberg.
Niemeyer, H., Skarmeta, J., Fuenzalida, R., Espinosa, W., 1984. Hojas Península de Taitao y Puerto Aisén. Región de Aisén del General Carlos Ibañez del Campo. Escala 1: 500.000. In: Servicio Nacional de Geología y Minería.
Pankhurst, R.J., Weaver, S.D., Hervé, F., Larrondo, P., 1999. Mesozoic-Cenozoic evolution of the North Patagonian batholith in Aysen, southern Chile. J. Geol. Soc. Lond. 156, 673–694.
Pérez, Y., 1999. Fuentes de aguas termales de la cordillera Andina del centro-sur de Chile (39 – 42°S). (Servicio Nacional de Geologia y Mineria).
Pérez-Flores, P., Cembrano, J., Sánchez-Alfaro, P., Veloso, E., Arancibia, G., Roquer, T., 2016. Tectonics, magmatism and paleo-fluid distribution in a strike-slip setting: insights from the northern termination of the Liquiñe-Ofqui fault System, Chile. Tectonophysics 680, 192–210.
Pulido-Leboeuf, P., 2004. Seawater intrusion and associated processes in a small coastal complex aquifer (Castell de Ferro, Spain). Appl. Geochemistry 19, 1517–1527.
Ramirez-Sánchez, E., Hervé, F., Kelm, U., Sassi, R., 2005. P-T conditions of metapelites from metamorphic complexes in Aysen, Chile. J. S. Am. Earth Sci. 19, 373–386.
Ray, M.C., Hilton, D.R., Muñoz, J., Fischer, T.P., Shaw, A.M., 2009. The effects of volatile recycling, degassing and crustal contamination on the helium and carbon geochemistry of hydrothermal fluids from the Southern Volcanic Zone of Chile. Chem. Geol. 266, 38–49.
Reyes, A.G., Christenson, B.W., Faure, K., 2010. Sources of solutes and heat in low-enthalpy mineral waters and their relation to tectonic setting, New Zealand. J. Volcanol. Geotherm. Res. 192, 117–141.
Risacher, F., Fritz, B., Hauser, A., 2011. Origin of components in Chilean thermal waters. J. S. Am. Earth Sci. 31, 153–170.
Sánchez, P., Pérez-Flores, P., Arancibia, G., Cembrano, J., Reich, M., 2013. Crustal deformation effects on the chemical evolution of geothermal systems: the intra-arc Liquiñe-Ofqui fault system, Southern Andes. Int. Geol. Rev. 55, 1384–1400.
Sanchez-Alfaro, P., Reich, M., Arancibia, G., Pérez-Flores, P., Cembrano, J., Driesner, T., Lizama, M., Rowland, J., Morata, D., Heinrich, C.A., et al., 2016. Physical, chemical and mineralogical evolution of the Tolhuaca geothermal system, southern Andes, Chile: insights into the interplay between hydrothermal alteration and brittle deformation. J. Volcanol. Geotherm. Res. 324, 88–104.
Sepúlveda, F., Dorsch, K., Lahsen, A., Bender, S., Palacios, C., 2004. Chemical and isotopic composition of geothermal discharges from the Puyehue-Cordón Caulle area (40.5° S), Southern Chile. Geothermics 33, 655–673.
Sepúlveda, F., Lahsen, A., Powell, T., 2007. Gas geochemistry of the Cordón Caulle geothermal system, Southern Chile. Geothermics 36, 389–420.
Sernageomin, 2010. Mapa Geológico de Chile: versión digital.
Sernageomin, 2011. Investigación Geológica Minera Ambiental en Aysen.
Srinivasamoorthy, K., Vasanthavigar, M., Chidambaram, S., Anandhan, P., Sarma, V.S., 2011. Characterisation of groundwater chemistry in an eastern coastal area of Cuddalore district, Tamil Nadu. J. Geol. Soc. India 78, 549–558.
Stallard, R.F., Edmond, J.M., 1983. Geochemistry of the Amazon: 2. The influence of geology and weathering environment on the dissolved load. J. Geophys. Res. Oceans 88, 9671–9688.
Suárez, M., De la Cruz, R., 2001. Jurassic to Miocene K-Ar dates from eastern central Patagonian Cordillera plutons, Chile (45° – 48°S). Geol. Mag. 138, 53–66.
Tanasković, I., Golobocanin, D., Miljević, N., 2012. Multivariate statistical analysis of hydrochemical and radiological data of Serbian spa waters. J. Geochem. Explor. 112, 226–234.
Tardani, D., Reich, M., Roulleau, E., Takahata, N., Sano, Y., Pérez-Flores, P., Sánchez-Alfaro, P., Cembrano, J., Arancibia, G., 2016. Exploring the structural controls on helium, nitrogen and carbon isotope signatures in hydrothermal fluids along an intra-arc fault system. Geochim. Cosmochim. Acta 184, 193–211.
Tassi, F., Martinez, C., Vaselli, O., Capaccioni, B., Viramonte, J., 2005. Light hydrocarbons as redox and temperature indicators in the geothermal field of El Tatio (northern Chile). Appl. Geochemistry 20, 2049–2062.
Tassi, F., Aguilera, F., Darrah, T., Vaselli, O., Capaccioni, B., Poreda, R.J., Huertas, A.D., 2010. Fluid geochemistry of hydrothermal systems in the Arica-Parinacota, Tarapacá and Antofagasta regions (northern Chile). J. Volcanol. Geotherm. Res. 192, 1–15.

Tonani, F.B., 1980. Some remarks on the application of geochemical techniques in geothermal exploration. In: Advances in European Geothermal Research. Springer, pp. 428–443.
Truesdell, A.H., Fournier, R.O., 1975. Calculation of Deep Temperatures in Geothermal Systems from the Chemistry of Boiling Spring Waters of Mixed Origin, in: Proc. Second UN Symposium on Geothermal Resources, San Francisco, CA, pp. 837–844.
Vengosh, A., 2003. Salinization and saline environments. In: Treatise on Geochemistry. Vol. 9. pp. 333–365.
Vengosh, A., Helvaci, C., Karamanderesi, I.H., 2002. Geochemical constraints for the origin of thermal waters from western Turkey. Appl. Geochem. 17, 163–183.
Willner, A.P., Hervé, F., Massonne, H.-J., 2000. Mineral chemistry and pressure-temperature evolution of two contrasting high-pressure-low-temperature belts in the Chonos Archipelago, Southern Chile. J. Petrol. 41, 309–330.